Supplement of Biogeosciences Discuss., 12, 13767–13791, 2015
http://www.biogeosciences-discuss.net/12/13767/2015/
doi:10.5194/bgd-12-13767-2015-supplement

Biogeosciences
Discussions
Open Access

Supplement of

Climate-driven shifts in continental net primary production implicated as a driver of a recent abrupt increase in the land carbon sink

W. Buermann et al.

Correspondence to: W. Buermann (w.buermann@leeds.ac.uk)

Supplement

This file includes:

Supplement Figures S1-S3

Supplement Tables S1-S2

Supplement Methods (incl. Figures S4-S8 and Table S3)

Supplement References

Supplement Figures

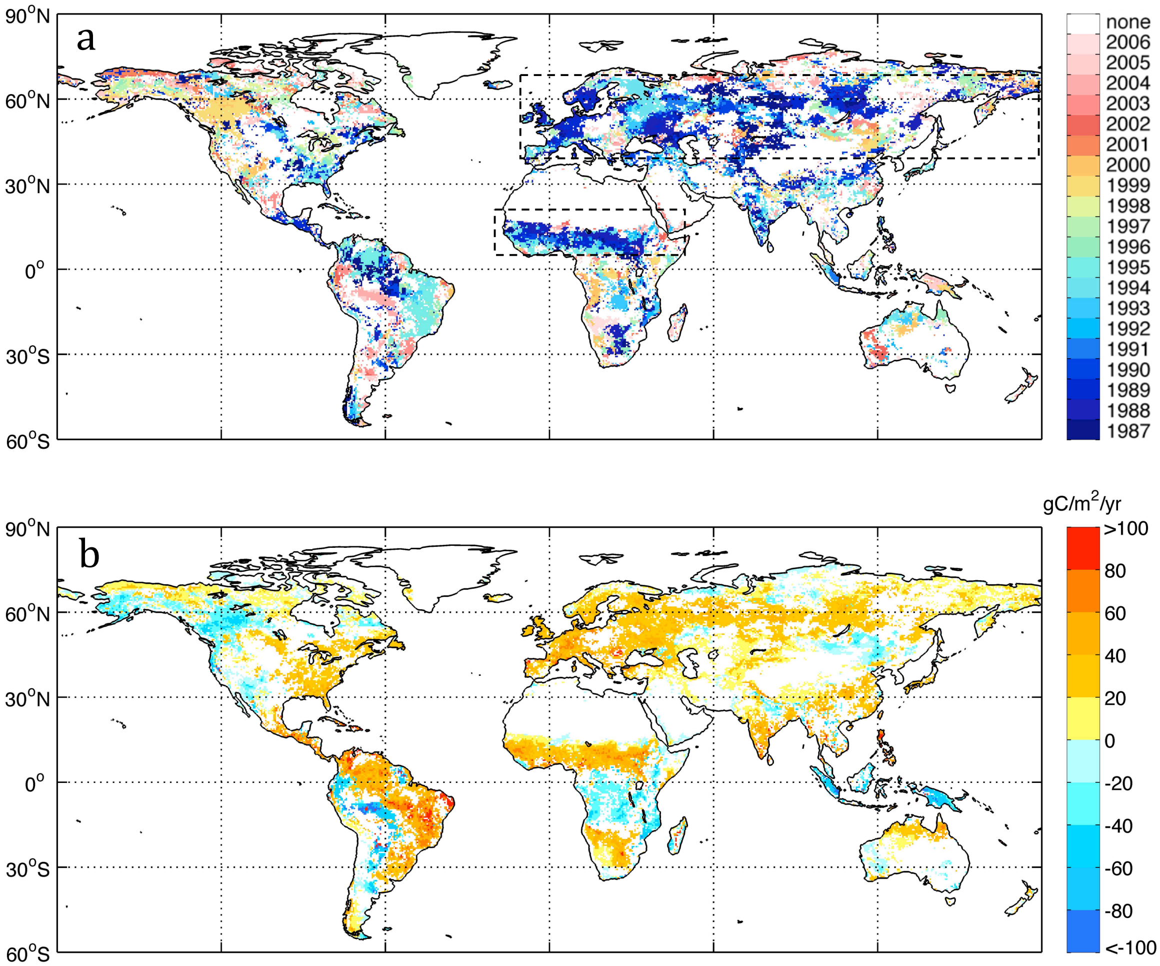

Figure S1. **Spatial pattern of abrupt shifts in data-driven NPP.** Maps show (a) timing and corresponding (b) direction and magnitude of abrupt shifts in data-driven (CASA) annual NPP in the satellite period 1982 to 2011. At each grid-point, three models were fitted including ‘constant mean’, ‘shift in the mean’ and ‘linear trend’ (see Section 2 in manuscript), and regions that are best represented by the ‘shift in the mean’ model are contoured. These results illustrate that for many land regions a ‘shift in the mean’ model fits terrestrial NPP dynamics over the roughly last 3 decades better than, for example, a linear trend. Further, many of the local shifts within the two target regions northern Eurasia and northern Africa (dashed rectangles in map (a)) are also statistically significant (see Fig. 1 in manuscript).

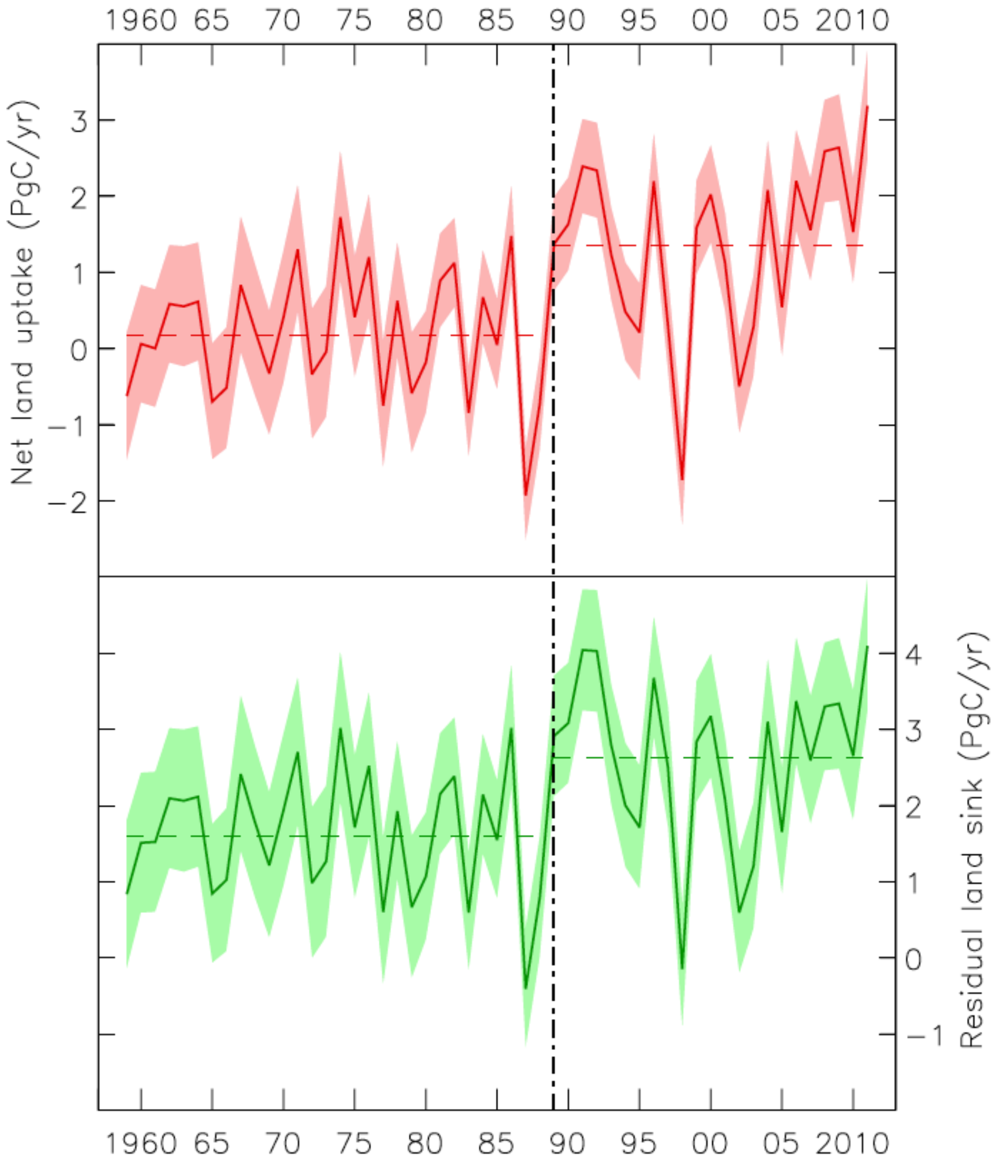

Figure S2. Temporal changes in global land-atmosphere carbon fluxes. Data are from the global carbon budget (Le Quéré et al., 2013; ref. in manuscript), and shaded contours represent 1σ uncertainties. In brief, the net land uptake (red) is inferred as the difference between fossil fuel emissions (estimated through inventories) and the sum of oceanic uptake (inferred through models subject to observational constraints) and atmospheric CO_2 growth rates (based on measurements). The 'residual' land sink (green) is then estimated as the difference between net land uptake and net LUC emissions (inferred trough a combination of techniques). Change point analysis with explicit accounting for uncertainties (see Methods in manuscript) shows that the 'residual' land sink and the net land uptake are best represented by a statistical model with a 'shift in the mean' in 1989 (dashed lines, see also Table 1 in manuscript). Taken together, these results confirm earlier results based on a less rigorous treatment of uncertainties in the global carbon budget (Beaulieu et al., 2012a; ref. in manuscript).

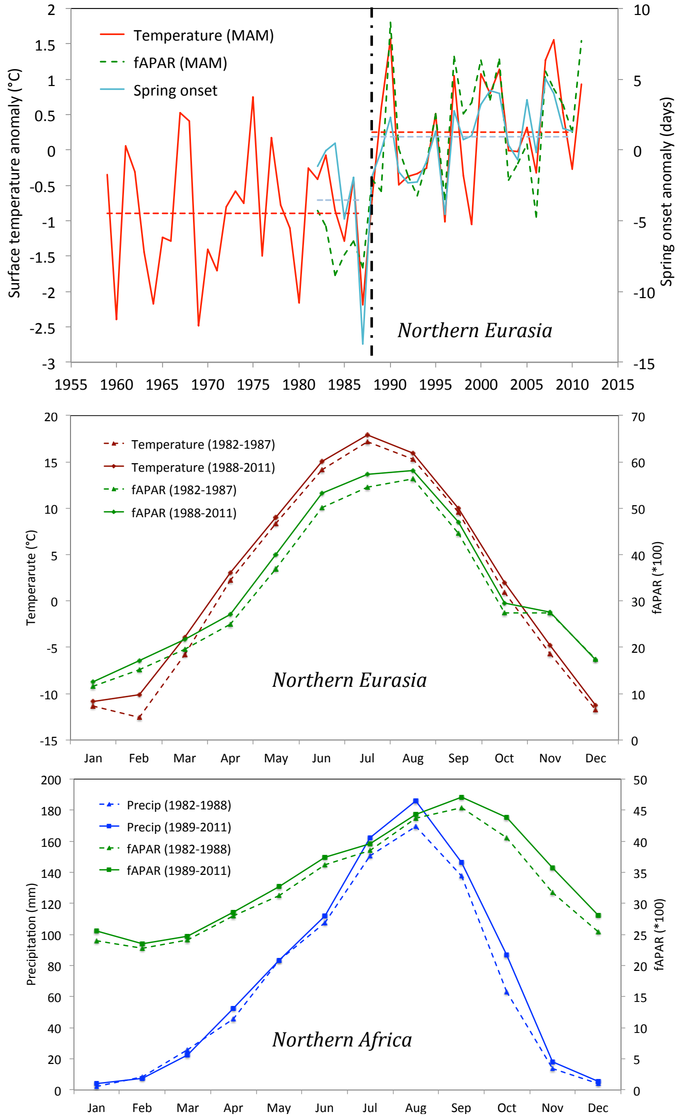

Figure S3. Interannual and seasonal changes in key forcing variables of data-driven NPP for northern Eurasia and northern Africa. Top panel shows spring (MAM) temperature and satellite fAPAR anomalies for the northern Eurasian target region plotted alongside anomalies in timing of spring onset (positive values correspond to earlier onset) representative of the same region and estimated through satellite microwave freeze-thaw data available for the period 1982-2010 (Kim et al., 2012). All anomalies are relative to 1982-2010. fAPAR data are scaled to allow visual comparisons. For the northern Eurasian region, interannual variations in the timing of spring onset as well as spring temperature and fAPAR are tightly coupled. Correlations between timing of spring onset and spring temperatures are r=0.84 (P<0.001), for timing of spring onset and spring fAPAR r=0.72 (P<0.001), and for spring temperatures and spring fAPAR r=0.79 (P<0.001), respectively. The drastic change in spring temperatures that accompanied the identified late 1980s NPP shift (see Table 1 in ms) is of the order of 1.2°C, whereas the timing of spring onset occurred about 5 days earlier in the period after the shift (dashed lines). The middle panel shows the seasonal cycles of satellite fAPAR and temperature representative of northern Eurasia for the periods prior and after the ‘1988’ shift, whereas the bottom panel shows the seasonal cycles of fAPAR and precipitation representative for northern Africa for the periods prior and after the ‘1989’ shift (see also Table 1 in manuscript).

Supplement Tables

Table S1. Timing and magnitude of abrupt changes in the terrestrial carbon cycle at global and continental scales. Shown are timing of the most likely shift (first data entry) along with associate magnitude (second data entry) and *P*-value (in brackets). Bold indicates shifts that are significant at the 5% critical level. The information shown is identical to the one shown in Table 1 in the manuscript, except that results are also shown for an additional test to assess the robustness of the identified shifts in which the two Pinatubo years (1992, 1993) were removed in the original time series prior change point analysis (No Pinatubo).

Region	Original data	Covariates[e]	No Pinatubo[f]
	Global Carbon Budget 1959-2011		
Residual land sink	**1989, +1.03 (0.003)**	**1989, +1.28 (<0.001)**	**1989, +1.06 (0.003)**
Net land uptake[d]	**1989, +1.19 (0.004)**	**1989, +1.43 (<0.001)**	**1989, +1.23 (0.001)**
	Data-driven (CASA) NPP 1982-2011		
Global	1995, +1.18 (0.239)[c]	1989, +1.12 (0.124)[c]	1989, +1.49 (0.084)[c]
Northern land (>30ºN)	**1988, +0.72 (0.010)**[c]	**1989, +0.62 (0.008)**[c]	**1988, +0.76 (0.003)**[c]
Tropic./south. land (<30ºN)	1995, +0.73 (0.266)[c]	1989, +0.50 (0.526)	1995, +0.70 (0.388)[c]
Northern Eurasia	**1988, +0.53 (<0.001)**[b]	**1989, +0.45 (0.001)**	**1988, +0.54 (<0.001)**[b]
Northern Africa	**1989, +0.20 (0.005)**	**1989, +0.17 (0.003)**	**1989, +0.21 (0.001)**
	Process-based (CASA) R_h 1982-2011		
Global	**1996, +0.96 (0.001)**	**1990, +0.80 (0.028)**[c]	**1996, +0.94 (0.001)**
Northern land (>30ºN)	**1990, +0.44 (0.003)**[c]	**1990, +0.42 (<0.001)**[a,c]	**1990, +0.46 (<0.001)**[c]
Tropic./south. land (<30ºN)	**1996, +0.63 (0.003)**	1996, +0.49 (0.054)	**1996, +0.61 (0.002)**
Northern Eurasia	**1988, +0.35 (0.004)**[a,c]	**1990, +0.29 (0.004)**[b,c]	**1988, +0.37 (<0.001)**[a,c]
Northern Africa	**1988, +0.18 (<0.001)**	**1991, +0.14 (0.003)**[b]	**1988, +0.19 (<0.001)**

a. Not normally distributed (Lilliefors test, 5% critical level)
b. Variance not constant (F-test, 5% critical level)
c. Residuals not independent (Kruskal-Wallis, 5% critical level)
d. Estimated as the difference between global fossil fuel emissions and the sum of atmospheric CO_2 growth rate and oceanic uptake
e. Variability related to ENSO and volcanic eruptions were removed in the original time series through regressions against the multivariate ENSO index and stratospheric optical thickness data as done in Beaulieu et al. (2012a); reference provided in manuscript
f. The two Pinatubo years (1992, 1993) were removed in the original time series prior change point analysis

Table S2. Timing and magnitude of abrupt changes in global and continental process-based NPP data, based on the TRENDY model ensembles. Results are for ensembles based on 9 models of the terrestrial biosphere that participated in TRENDY (ref. 13 in manuscript) and experiments in which climate and CO_2 driver data (S2) as well as climate driver data only (S2-S1) were varied (see also Methods in ms). Shown are timing of the most likely shift (first data entry) along with associate direction and magnitude (second data entry) and *P*-value (in brackets). Magnitude and *P*-values are only provided if the 'shift in the mean model' was more likely than a 'linear trend' or 'constant mean' model. The timing of a shift captures the first year of a new regime. The *P*-values are obtained using Monte Carlo simulations that take into account uncertainty in the original data. Bold indicates shifts that are significant at the 5% critical level.

Region	Original data	Covariates[e]	No Pinatubo[f]
Process-based (TRENDY) NPP 1982-2010 - Climate varied only (S2 – S1)			
Global	1996[d]	**1990, +0.81 (0.016)**	1989[d]
Northern land (>30ºN)	**1990, +0.51 (0.001)**[b]	**1989, +0.50 (0.002)**	**1990, +0.53 (0.004)**[b]
Tropic./south. land (<30ºN)	1996, +0.76 (0.061)	1996, +0.52 (0.087)	1996, +0.76 (0.112)
Northern Eurasia	**1988, +0.26 (0.004)**[a]	1988, +0.26 (0.098)	**1988, +0.28 (0.003)**[a]
Northern Africa	**1988, +0.27 (0.001)**	**1991, +0.30 (0.003)**[a]	**1988 +0.30 (<0.001)**[a]
Process-based (TRENDY) NPP 1959-2010 - Climate varied only (S2 – S1)			
Global	1998, +0.79 (0.109)	**1973, +0.75 (0.019)**[b,c]	1998, **+0.77** (0.138)
Northern land (>30ºN)	**1990, +0.55 (<0.001)**	**1990, +0.54 (<0.001)**	**1990, +0.59 (<0.001)**
Tropic./south. land (<30ºN)	1979[e]	1972, +0.51 (0.163)	1979[e]
Northern Eurasia	**1988, +0.25 (<0.001)**	**1988, +0.24 (0.001)**	**1988, +0.27 (<0.001)**
Northern Africa	**1969, -0.24 (0.038)**[b,c]	1970, -0.21 (0.077)[b,c]	**1969 -0.24 (0.044)**[b,c]
Process-based (TRENDY) NPP 1982-2010 - Climate and CO_2 varied (S2)			
Global	1997[d]	1997[d]	1996[d]
Northern land (>30ºN)	1997[d]	1990[d]	1990[d]
Tropic./south. land (<30ºN)	1996[d]	1996[d]	1996[d]
Northern Eurasia	1990[d]	1990[d]	1990[d]
Northern Africa	1988[d]	**1991, +0.44 (<0.001)**	1991[d]
Process-based (TRENDY) NPP 1959-2010 - Climate and CO_2 varied (S2)			
Global	1996[d]	1989[d]	1989[d]
Northern land (>30ºN)	1990[d]	1990[d]	1990[d]
Tropic./south. land (<30ºN)	1996[d]	1991[d]	1996[d]
Northern Eurasia	1988[d]	1988[d]	1988[d]
Northern Africa	**1994, +0.30 (<0.001)**[c]	**1991, +0.32 (<0.001)**[c]	**1991, +0.31 (0.001)**[c]

a. Not normally distributed (Lilliefors test, 5% critical level)

b. Variance not constant (F-test, 5% critical level)

c. Residuals not independent (Kruskal-Wallis, 5% critical level)

d. ‘Linear trend’ model fits data better than a ‘shift in the mean’ model, hence shift magnitude and *P*-value is not calculated

e. Variability related to ENSO and volcanic eruptions were removed in the original time series through regressions against the multivariate ENSO index and stratospheric optical thickness data as done in Beaulieu et al. (2012a); reference provided in manuscript

f. The two Pinatubo years (1992, 1993) were removed in the original time series prior change point analysis

Supplement Methods

Evaluation of Key Driver Datasets for CASA Simulations

The CASA model is forced by temporally varying estimates of fAPAR, near surface air temperature, precipitation and incoming surface solar radiation at monthly time steps at a spatial resolution of 0.5º. While high-resolution gridded temperature data (CRU TS3.21) are considered relatively robust, uncertainties in global fAPAR, precipitation and solar radiation datasets are potentially large and need to be accounted for in the model simulations. For our study period 1981-2011 available data for satellite-based fAPAR are limited to one dataset (FPAR3g; see manuscript). For precipitation and solar radiation multiple datasets exist, and we evaluated a set of candidate datasets (Table S3). The ISCCP solar radiation dataset was removed from further consideration because it was found to be biased high over the Amazon (see below). All combinations of the remaining three solar radiation and three precipitation datasets (Table S3) were used to force the CASA model to produce an ensemble of nine simulations.

<u>Surface Shortwave Radiation</u>

We analyzed three satellite remote sensing and one empirically based estimate of global surface incoming shortwave radiation (Table S3). The satellite-based datasets extend from 1983-2007 as limited by the availability of satellite cloud data and here we use the full years of data (1984-2007). The empirical dataset (Sheffield et al., 2006), which is available for the full time period, is also used to extend the satellite-based datasets to 1982-2011 using pdf matching. All datasets are available at 3-hour resolution and are averaged to monthly means to force the CASA model.

Table S3. Surface downward solar radiation and precipitation datasets.

Dataset	Time period	Domain	Source	Reference
Solar Radiation				
ISCCP FD-SRF*	1984-2007	Global, 280km	Satellite	Zhang et al. (2004)
SRB V3	1984-2007	Global, 1.0deg	Satellite	Stackhouse et al. (2011)
UMD	1983-2007	Global, 0.5deg	Satellite	Mao and Pinker (2012)
PGF	1948-2011	Global, 1.0deg	Empirical (cloud cover)	Sheffield et al. (2006)
Precipitation				
CRU TS3.2	1901-2013	Global, 0.5-deg	Station	Harris et al. (2014)
UDel V3.01	1900-2010	Global, 0.5-deg	Station	Willmott and Matsuura (2012)
GPCP V2.2	1979-2012	Global, 2.5-deg	Satellite/station	Huffman et al. (2009)

*Not included in CASA simulations

a) International Satellite Cloud Climatology Project (ISCCP)

The ISCCP FD-SRF surface solar radiation flux data are calculated using the NASA Goddard Institute for Space Studies (GISS) radiation transfer model based on ISCCP satellite visible and infrared radiances and cloud properties, and the TIROS Operational Vertical Sounder (TOVS) atmospheric temperature and humidity profiles. The ISCCP cloud data are sampled from multiple geostationary and polar orbiting sensor retrievals which have reasonable spatial and temporal sampling for clear and cloudy conditions, but may suffer from inconsistencies in time due to changes in sensor view angles (Evan et al., 2007).

b) Surface Radiation Budget (SRB)

The current version (V3) of the SRB includes estimates of surface radiation components available at 3-hourly and 1.0 degree (~100km) resolution for 1983-2007. The SRB data have explicit representations of aerosols, including dust and black carbon, which, although there remain considerable uncertainties in their distribution and effects, are important factors in regional climate and its terrestrial impacts via changes in available radiation. The fluxes are computed with two retrieval algorithms: a 'primary' (SRB) and 'quality-check' (SRBqc) and we use the SRB dataset here. The retrievals use temperature and water vapor profiles from the Goddard Earth Observing System (GEOS-4) (Bloom et al., 2005) and satellite visible and infrared radiances and cloud properties from the ISCCP pixel level (DX) data.

c) University of Maryland (UMD)

The UMD dataset of Ma and Pinker (2012) is a relatively new global dataset of surface fluxes at 0.5-degree, 3-hourly resolution for 1983 to 2007. These have been generated with V3.3.3 of the UMD/SRB model using ISCCP DX satellite cloud data. This upgrades the previous version of the UMD/SRB model by incorporating new auxiliary information for land cover, improved aerosol treatment and separation of clouds by phase.

d) Princeton Global Forcings (PGF)

The empirical dataset of Sheffield et al. (2006) is based on regressions between monthly downward surface solar radiation and cloud cover developed from the NCEP/NCAR reanalysis (Kalnay et al., 1996) and applied to the observational gridded cloud cover analysis from the CRU TS3.1 dataset (Harris et al. 2014). The values are then scaled to match the climatological values of the UMD dataset. The dataset does not include the direct effect of aerosols and is subject to the uncertainties in the regression relationships and the reliability of the CRU cloud data (Harris et al., 2014). The latter are based on station cloud observations taken from the CRU TS2.0 dataset up to 2002, and then derived using relationships with diurnal temperature range thereafter.

e) Comparison of solar radiation datasets and evaluation against GEBA station observations

Figures S4-S5 compare the four solar radiation datasets against station observations from the Global Energy Balance Archive (GEBA; Gilgen and Ohmura, 1999). The GEBA contains monthly mean surface radiation flux data for several thousand stations worldwide, with some station records back to 1922. We compare the data for the period 1984-2007 and when GEBA data have more than 10 years of data over this period. Under this criterion, data for 510 GEBA stations are available, which are mainly located in western Europe and east Asia with very few stations over the focus regions of this study. The dataset biases tend to be positive relative to the GEBA stations with the largest biases of the order of 20-50 W/m^2 over east Asia and northern South America/Caribbean (Figures S4). Correlations between gridded solar radiation and station data (Figure S5) are calculated on the monthly anomalies to remove the seasonal cycle. The correlations are mostly higher than 0.5 and are largest in western Europe and some stations in N. America, east Asia and Australia, with correlations > 0.9. The mean correlation across stations is similar for the satellite based datasets but slightly lower for the empirical dataset (mean correlation: ISCCP = 0.70; SRB = 0.69; UMD = 0.71; PGFemp = 0.59) likely because the empirical dataset does not include direct aerosol effects. The correlations are lowest (< 0.4) at isolated stations across the world, and for nearly all stations in northern South America.

Figure S6 shows the annual and monthly times series of solar radiation for the four datasets averaged over the two focus regions northern Eurasia and northern Africa. These regions have very few GEBA stations with available data for our time period and so a comprehensive evaluation against observations is not possible. The data are reasonably well matched in terms of the absolute values and the correlation over time, although there are several aspects of disagreement. The ISCCP and SRB datasets are well correlated over the three regions, but the UMD and PGFemp datasets tend to diverge, especially in the last 10 years. Complementary analysis shows that across the Amazon, the ISCCP dataset is about 15 W/m^2 higher than the other datasets (results not shown), which are likely biased high based on the few GEBA comparisons in the far northern part of South America (Figure S4). Because of this and the fact that the ISCCP dataset are well correlated with the SRB data (and hence does not provide independent information) we did not use the ISCCP data in the CASA simulations.

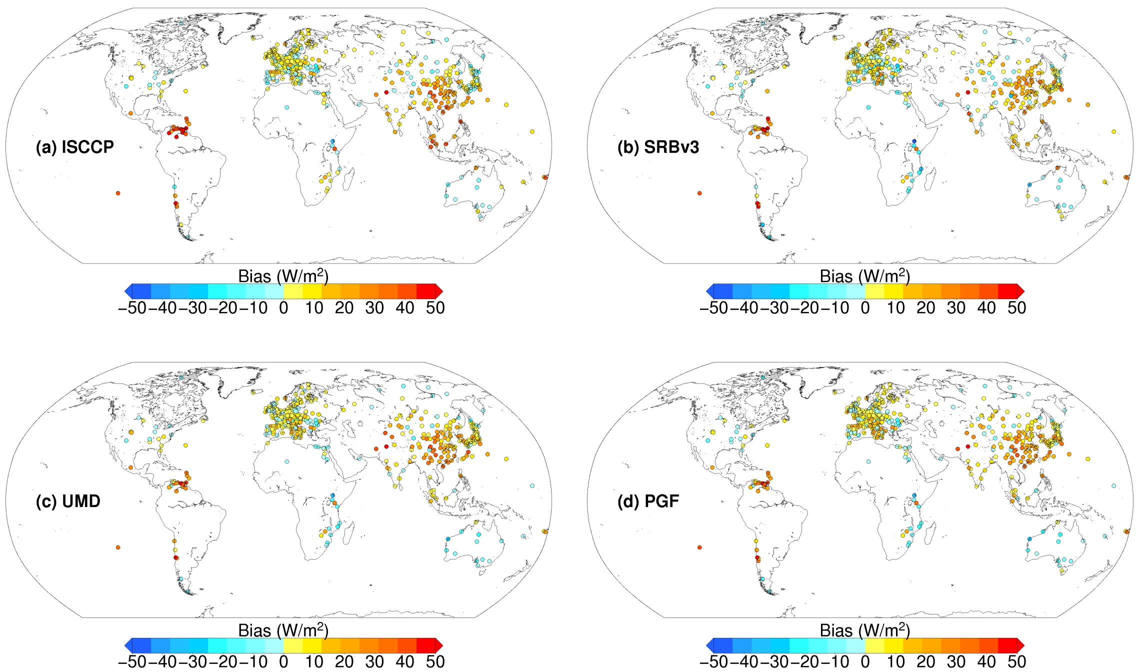

Figure S4. Mean bias in downward surface solar radiation (dataset minus GEBA) for the three satellite datasets (a-c) and the empirical dataset (d). Biases are calculated for time periods with available stations data between 1984-2007. The number of records varies between GEBA stations, but a station is only used when a minimum of 10 years of data are available.

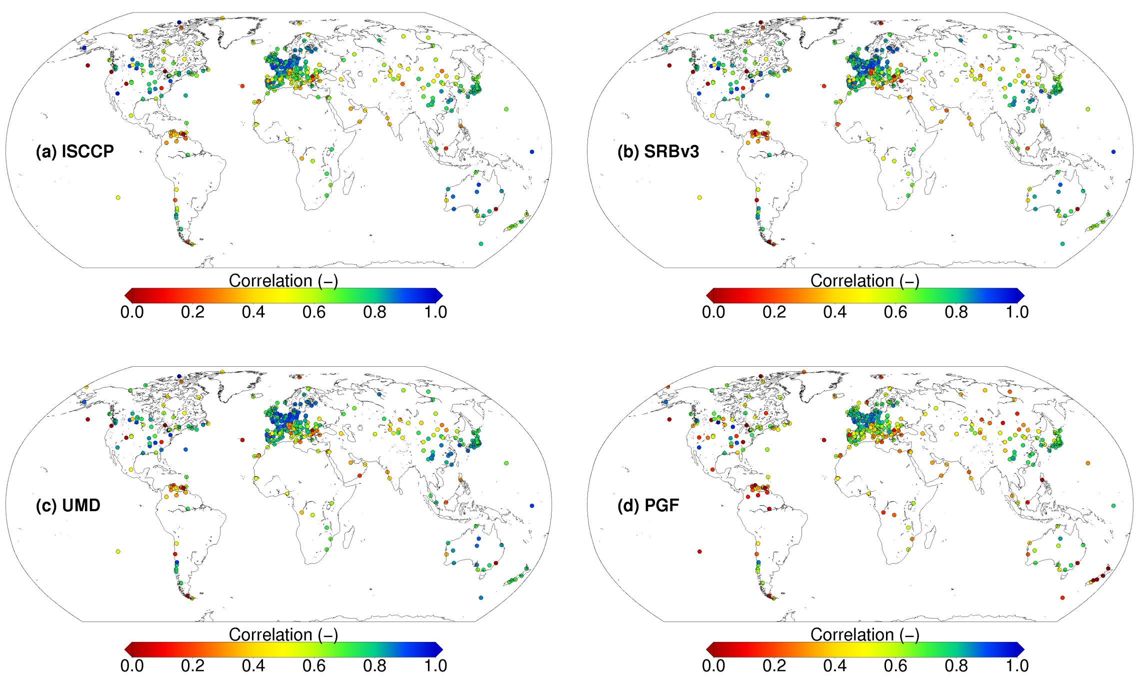

Figure S5. As Figure S4, but for the correlation between the GEBA station data and the three satellite-based datasets (a-c) and the empirical dataset (d).

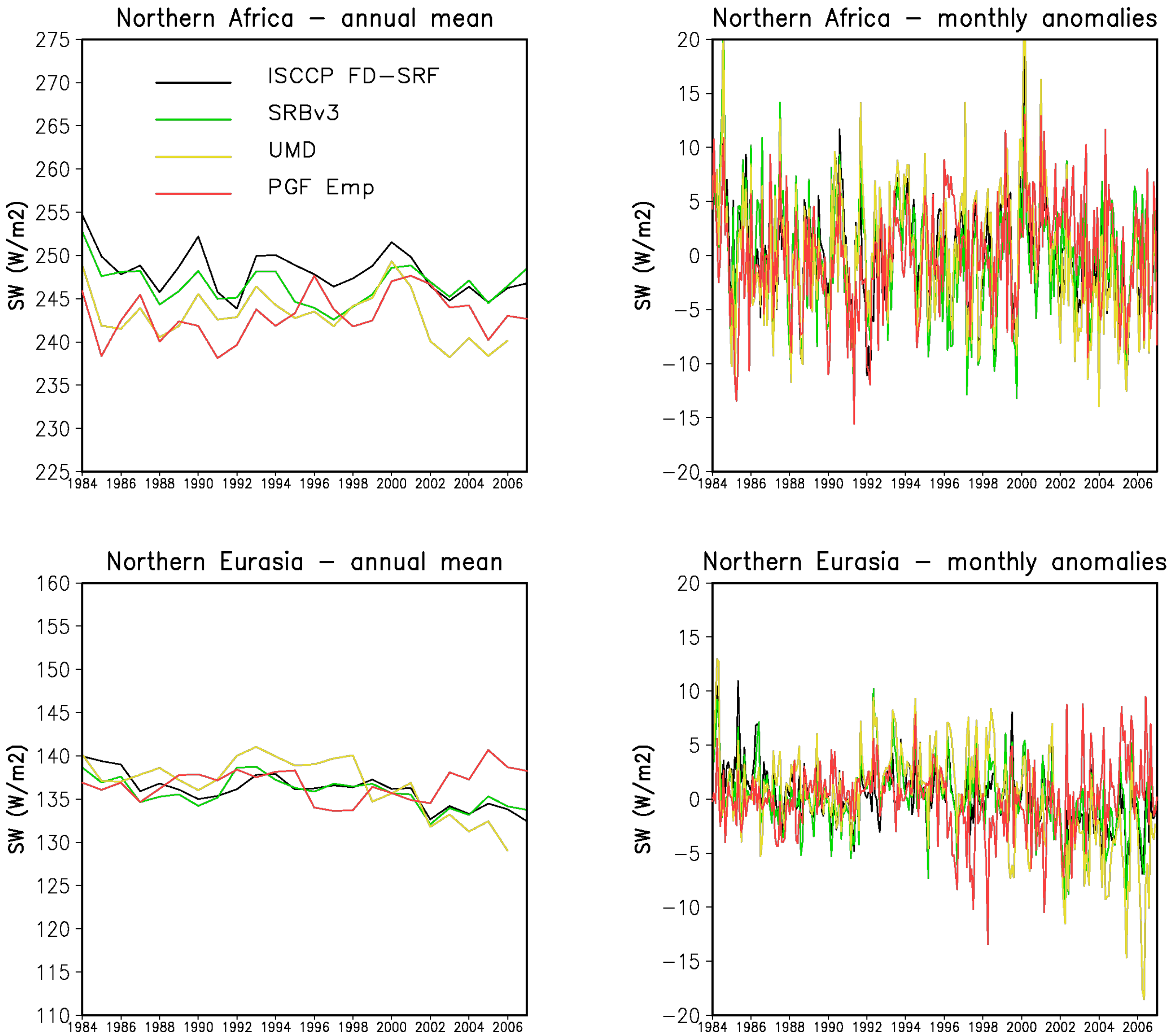

Figure S6. Regional average time series of downward surface solar radiation for (left) annual means and (right) monthly anomalies. Regions are as defined in the manuscript (see Figure 1).

Precipitation

We estimate uncertainties in precipitation by evaluating three global precipitation datasets (Table S3). These datasets are based on gauge measurements that are interpolated to a grid, and in the case of the GPCP dataset merged with satellite estimates. The datasets differ in the set of gauges that they use and the methods for quality-controlling the data and interpolating to a grid. The differences among datasets are shown in Figure 5 in terms of the global land averaged time series and the number of gauges contributing to each dataset. Figure 6 shows the time series averaged over the focus regions.

a) University of Delaware (UDel)

This dataset is mainly based on station measurements from the quality-controlled monthly values from the Global Historical Climatology Network (GHCN2) database, but is merged with data from other global and regional datasets, with between 4100 to 22000 stations used globally each year. No adjustment is made for raingauge undercatch. Station values were interpolated to 0.5-degree resolution using climatologically aided interpolation (CAI) (Willmott and Robeson, 1995), which uses a background climatology taken from Legates and Willmott (1990). The climatology is used to calculate differences at each station, which were then interpolated to the grid and added back to the gridded climatology. Interpolation was done using a spherical version of Shepard's algorithm, which employs an enhanced distance-weighting method (Shepard, 1968; Willmott et al., 1985).

b) Climatic Research Unit (CRU)

The CRU (V3.2) data (Harris et al., 2014) are based on CLIMAT records and Monthly Climatic Data for the World (MCDW) obtained from the World Meteorological Organization (WMO) via the US National Climatic Data Center (NCDC) with the number of stations included varying from year to year with a maximum of about 2800. These are supplemented or replaced in some cases by regional quality-controlled datasets where available. A similar method to the U. Delaware dataset is used to produce gridded anomalies, but using percentages. Interpolation is based on correlation decay distances, which is about 450km for precipitation and using climatology where no nearby stations are available. Triangular linear interpolation is used to grid the anomalies. Comparisons with the Global Precipitation Climatology Centre (GPCC; Schneider et al., 2013) V5 shows a mean regional correlation of 0.89 with differences greater since the late 1990s in Alaska, Central America, and all African regions.

c) Global Precipitation Climatology Project (GPCP)

The GPCP dataset (Adler et al., 2003; Huffman et al., 2009) merges satellite precipitation retrievals with gauge climatology. Passive microwave estimates from the Special Sensor Microwave/Imager (SSMI) and Special Sensor Microwave Imager/Sounder (SSMIS) and infrared (IR) precipitation estimates from primarily U.S., European and Japanese geostationary satellites and secondarily from NOAA-series polar-orbiting satellites. Precipitation estimates are also used from the Atmospheric Infrared Sounder (AIRS) data from the NASA Aqua, and Television Infrared Observation Satellite Program (TIROS) Operational Vertical Sounder (TOVS) and Outgoing Longwave Radiation (OLR) Precipitation Index (OPI) data. These estimates are combined with the Global Precipitation Climatology Centre (GPCC) climatology to provide a 2.5-degree gridded dataset. We interpolated the data to 0.5-degree for the CASA simulations.

d) Comparison of precipitation datasets

Figure S7 compares the three precipitation datasets in terms of global land time series of annual mean and anomalies, and the number of contributing stations. The GPCP dataset is higher globally than the other two datasets, which is partly because it adjusts for gauge undercatch, which mainly increases values in wintertime over high latitudes (Figure S7a). The anomalies are well correlated globally with the CRU dataset tending to have a positive trend in recent years (Figure S7b). Regionally the differences are highest across southeast Asia and the Indonesian islands, central America, parts of northwestern South America and the Pacific northwest of North America (Figure S7c), which aligns with the regions of lowest gauge density, particularly for the CRU dataset (Figure S7e,f). For the GPCP dataset, the satellite precipitation estimates are merged with the GPCC station analysis (Schneider et al., 2013) and so we show the station count for the GPCC dataset. The number of stations used by the CRU dataset is about 10% of that used by the GPCC since the 1980s (Figure S7d), although the GPCC station count is very dense in a few countries and the CRU stations tend to have long term records and therefore the CRU datasets may be more temporally homogeneous. The station count for the UDel dataset is not available but ranges between 4100 and 22000 stations per year and we assume that this is somewhere between the GPCC and CRU station counts. The number of stations contributing to each dataset has declined rapidly since the 1980s, and this has increased the differences between the datasets relative to the period of highest densities (1960s-1970s; not shown). Regionally the datasets are

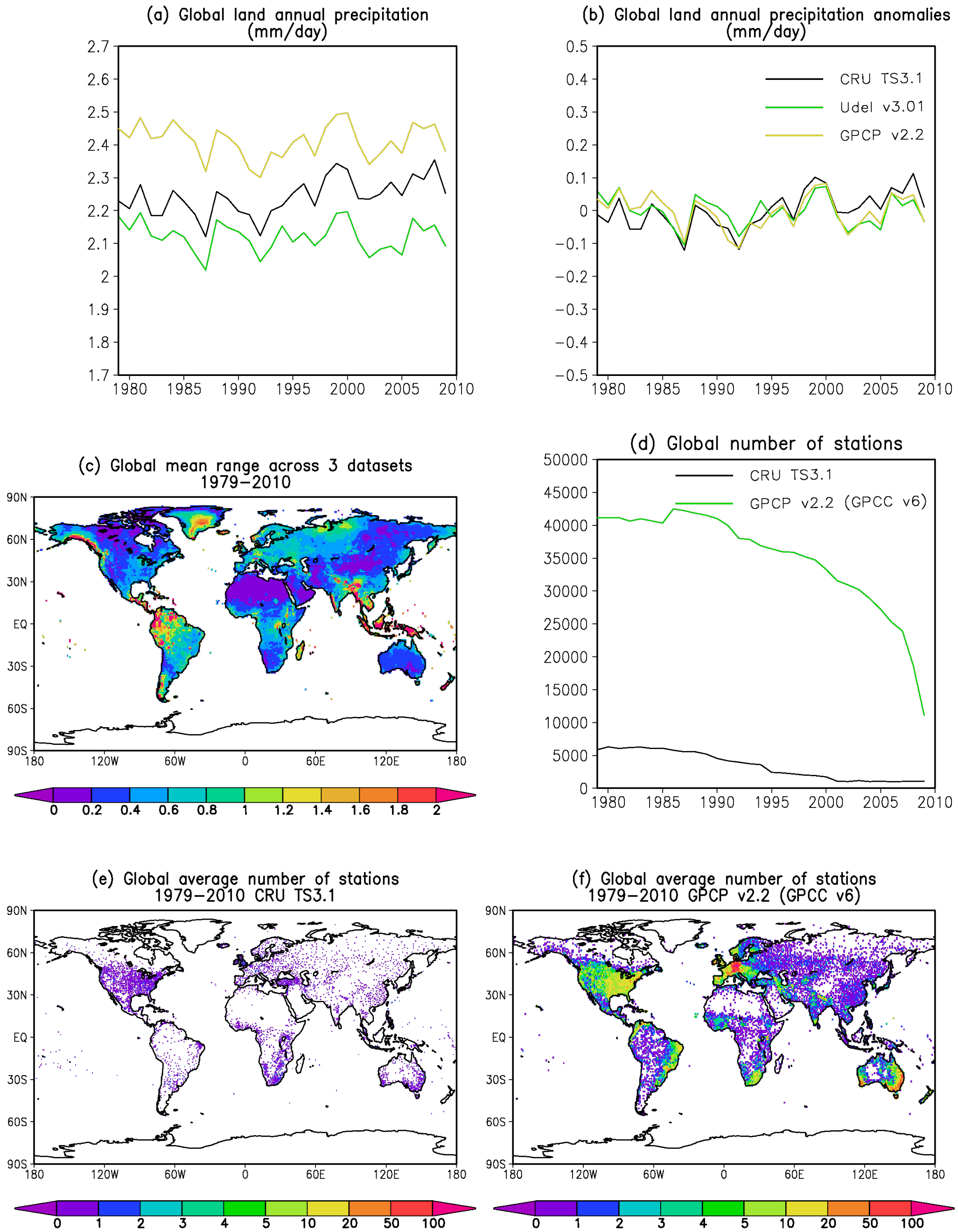

Figure S7. (a) Time series of annual mean precipitation (mm/day) averaged over land areas excluding Antarctica for the three precipitation datasets. (b) As (a) but for annual anomalies relative to 1979-2010. (c) Mean range in annual precipitation across the three datasets (mm/day). (d) Number of stations that contributed to the datasets. The GPCP datasets] is merged with station estimates from the GPCC dataset. No information is available on the number of stations for the UDel dataset. (e) Global distribution of the average number of stations for CRU TS3.1 for 1979-2010. (f) As (e) but for the GPCP v2.2 (based on GPCC v6).

very similar (Figure S8) with a slight divergence by the CRU dataset in recent years and higher values in the GPCP in northern Eurasia because of the gauge undercatch correction.

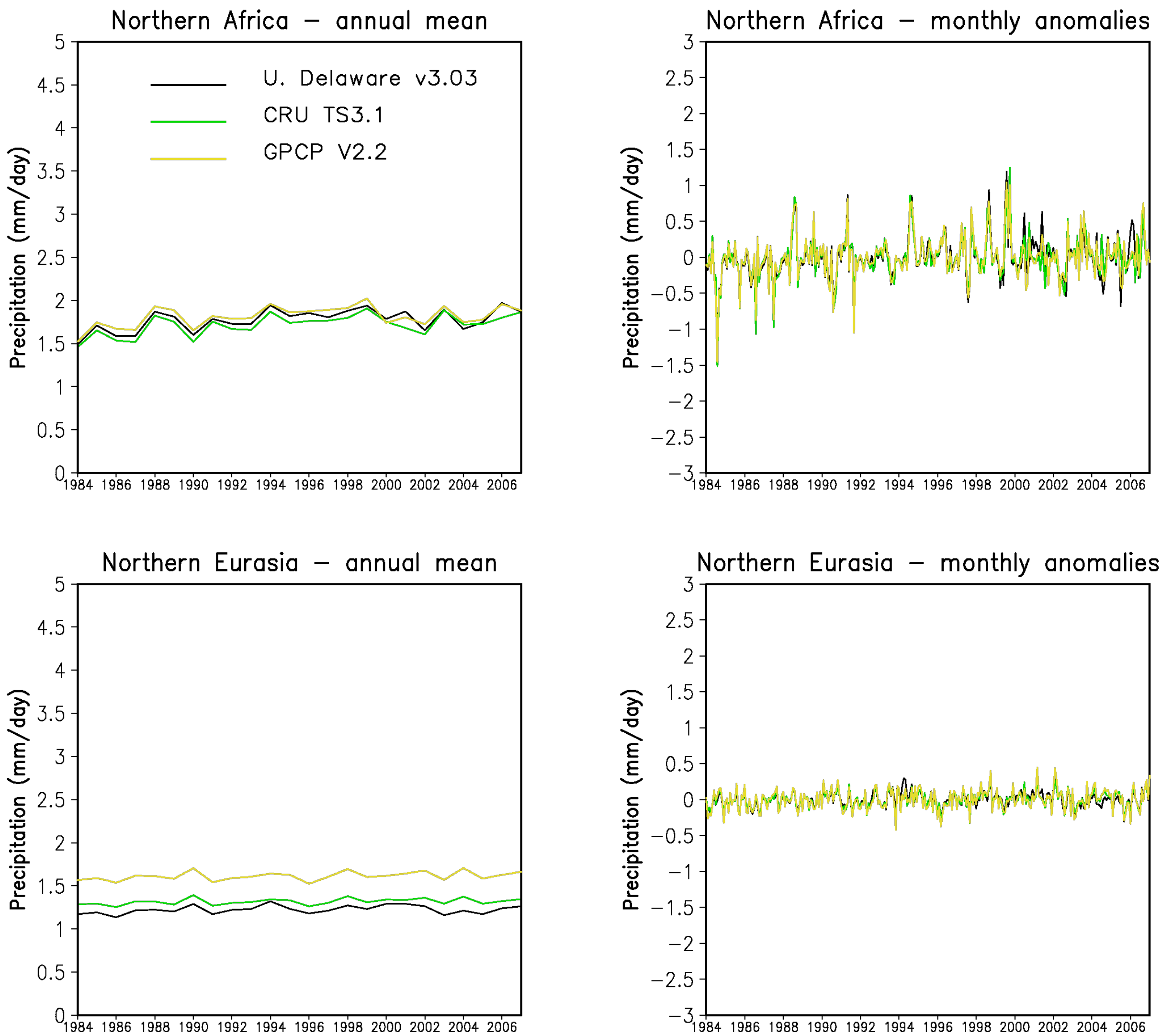

Figure S8. Regional average time series of precipitation for (left) annual means and (right) monthly anomalies. Regions are as defined in the manuscript (see Fig. 1).

Supplement References

Adler, R.F., G.J. Huffman, A. Chang, R. Ferraro, P. Xie, J. Janowiak, B. Rudolf, U. Schneider, S. Curtis, D. Bolvin, A. Gruber, J. Susskind, P. Arkin, E. Nelkin 2003: The Version 2 Global Precipitation Climatology Project (GPCP) Monthly Precipitation Analysis (1979-Present). J. Hydrometeor., 4,1147-1167.

Enfield, D.B., A.M. Mestas-Nunez, and P.J. Trimble (2001) The Atlantic Multidecadal Oscillation and its relationship to rainfall and river flows in the continental U.S., Geophys. Res. Lett., 28: 2077-2080.

Evan, A.T, A.K. Heidinger and D.J. Vimont (2007) Arguments against a physical long-term trend in global ISCCP cloud amounts. Geophys. Res. Lett. 34, L04701.

Gilgen, H. and A. Ohmura (1999) The Global Energy Balance Archive (GEBA). *Bull. Am. Met. Soc.,* 80, 831-850.

Harris, I., Jones, P.D., Osborn, T.J. and Lister, D.H. (2014), Updated high-resolution grids of monthly climatic observations – the CRU TS3.10 Dataset. Int. J. Climatol., 34: 623–642.

Hoerling, M.J., J. Hurrell, J. Eischeid, and A. Phillips (2006) Detection and attribution of 20th century Northern and Southern African rainfall change. J. Clim. 19, 3989–4008.

Huffman, G.J, R.F. Adler, D.T. Bolvin, and G. Gu (2009) Improving the Global Precipitation Record: GPCP Version 2.1. Geophys. Res. Lett., 36, L17808.

Hurrell, J.W. (1995) Decadal trends in the North Atlantic oscillation regional temperatures and precipitation. Science 269, 676–679.

Kalnay, E., and Coauthors, (1996) The NCEP/NCAR 40-Year Reanalysis Project. Bull. Amer. Meteor. Soc., 77, 437–471.

Kim Y, J.S. Kimball, K. Zhang and K.C. McDonald (2012) Satellite detection of increasing Northern Hemisphere non-frozen seasons from 1979 to 2008: implications for regional vegetation growth. Remote Sens. Environ. 121 472–87.

Legates, D. R. and C. J. Willmott (1990). Mean seasonal and spatial variability in gauge-corrected, global precipitation. International Journal of Climatology, 10, 111-127.

Le Quéré , C., et al. (2009) Trends in the sources and sinks of carbon dioxide, Nat. Geosci. 2, 831–836.

Ma, Y., and R. T. Pinker (2012), Modeling shortwave radiative fluxes from satellites, J. Geophys. Res., 117, D23202.

Schneider, U. et al (2013): GPCC's new land surface precipitation climatology based on quality-controlled in situ data and its role in quantifying the global water cycle. Theoretical and Applied Climatology http://dx.doi.org/10.1007/s00704-013-0860-x

Sheffield, J., G. Goteti, and E.F. Wood (2006) Development of a 50-yr high-resolution global dataset of meteorological forcings for land surface modeling, J. Climate, 19, 3088-3111.

Shepard, D. (1968). A two-dimensional interpolation function for irregularly-spaced data. Proceedings, 1968 ACM National Conference, 517-523.

Stackhouse, Jr., P.W., et al. (2011) The NASA/GEWEX Surface Radiation Budget Release 3.0: 24.5-Year Dataset. GEWEX News, 21, 10-12.

Thompson, D.W.J. & J.M. Wallace (1998) The Arctic oscillation signature in the wintertime geopotential height and temperature fields. Geophys. Res. Lett. 25, 1297–1300.

Willmott, C.J. and S.M. Robeson (1995). Climatologically aided interpolation (CAI) of terrestrial air temperature. International Journal of Climatology, 15(2), 221-229.

Willmott, C. J., C. M. Rowe and W. D. Philpot (1985). Small-scale climate maps: a sensitivity analysis of some common assumptions associated with grid-point interpolation and contouring. American Cartographer, 12, 5-16.

Willmott, C. J. and K. Matsuura (2012) Terrestrial Air Temperature and Precipitation: Monthly and Annual Time Series (1900 - 2010), http://climate.geog.udel.edu/~climate/html_pages/Global2011/README.GlobalTsP2011.html.

Zhang, Y., et al. (2004), Calculation of radiative fluxes from the surface to top of atmosphere based on ISCCP and other global data sets: Refinements of the radiative transfer model and the input data. J. Geophys. Res., 109, D19105.